

This document is confidential and is proprietary to the American Chemical Society and its authors. Do not copy or disclose without written permission. If you have received this item in error, notify the sender and delete all copies.

Trapping of Charged Gold Adatoms by Dimethyl Sulfoxide on a Gold Surface

Journal:	<i>ACS Nano</i>
Manuscript ID:	nn-2015-02284x.R2
Manuscript Type:	Article
Date Submitted by the Author:	n/a
Complete List of Authors:	Feng, Zhijing; University of Trieste, Department of Physics; IOM-CNR Laboratorio TASC, Velari, Simone; University of Trieste, Engineering and Architecture Department Cossaro, Albano; IOM-CNR Laboratorio TASC, Castellarin-Cudia, Carla; IOM-CNR Laboratorio TASC, verdini, alberto; IOM - Istituto Officina dei Materiali, Vesselli, Erik; University of Trieste, Department of Physics; IOM-CNR Laboratorio TASC, Dri, Carlo; University of Trieste, Department of Physics; IOM-CNR Laboratorio TASC, Peressi, Maria; University of Trieste, Department of Physics; IOM-CNR DEMOCRITOS, ; Consorzio Interuniversitario Nazionale per la Scienza e la Tecnologia dei Materiali (INSTM), Unità di ricerca di Trieste De Vita, Alessandro; University of Trieste, Engineering and Architecture Department; King's College London, Physics Comelli, Giovanni; University of Trieste, Department of Physics; IOM-CNR Laboratorio TASC,

SCHOLARONE™
Manuscripts

Trapping of Charged Gold Adatoms by Dimethyl Sulfoxide on a Gold Surface

Zhijing Feng,^{†,¶} Simone Velari,[‡] Albano Cossaro,[¶] Carla Castellarin-Cudia,[¶] Alberto Verdini,[¶]
Erik Vesselli,^{†,¶} Carlo Dri,^{†,¶} * Maria Peressi,^{†,⊥,||} Alessandro De Vita,^{‡,§} and Giovanni
Comelli^{†,¶}

[†]Physics Department, University of Trieste, Via A. Valerio 2, 34127 Trieste, Italy

[‡]Engineering and Architecture Department, University of Trieste, Via A. Valerio 6/1, 34147
Trieste, Italy

[¶]TASC Laboratory, Istituto Officina dei Materiali IOM-CNR, S.S. 14 km 163,5, 34149 Trieste,
Italy

^{||}IOM-CNR DEMOCRITOS, Area Science Park, S.S. 14 km 163,5, 34149 Trieste, Italy

[⊥]Consorzio Interuniversitario Nazionale per la Scienza e la Tecnologia dei Materiali (INSTM),
Unità di ricerca di Trieste, Piazzale Europa 1, 34128 Trieste, Italy,

[§]King's College London, Department of Physics, Strand, London WC2R 2LS, United Kingdom

KEYWORDS: dimethyl sulfoxide, DMSO, scanning tunneling microscopy, photoemission
spectroscopy, density functional theory, gold, adatom

1
2
3 ABSTRACT We report the formation of Dimethyl Sulfoxide (DMSO) molecular complexes on
4
5 Au(111) enabled by native gold adatoms unusually linking the molecules *via* a bonding of ionic
6
7 nature, yielding a mutual stabilization between molecules and adatom(s). DMSO is a widely
8
9 used polar, aprotic solvent whose interaction with metal surfaces is not fully understood. By
10
11 combining X-ray photoelectron spectroscopy, low temperature scanning tunneling microscopy,
12
13 and density functional theory (DFT) calculations, we show that DMSO molecules form
14
15 complexes made by up to four molecules arranged with adjacent oxygen terminations. DFT
16
17 calculations reveal that most of the observed structures are accurately reproduced if, and only if,
18
19 the negatively charged oxygen terminations are linked by one or two positively charged Au
20
21 adatoms. A similar behavior was previously observed only in non-stoichiometric organic salt
22
23 layers, fabricated using linkage alkali atoms and strongly electronegative molecules. These
24
25 findings suggest a motif for anchoring organic adlayers of polar molecules on metal substrates
26
27 and also provide nanoscale insight into the interaction of DMSO with gold.
28
29
30
31
32
33
34
35

36 The ability to control the structural and electronic properties of (hetero-)organic assemblies on
37
38 metal surfaces is the key issue for the design of efficient devices in organic electronics, which
39
40 has triggered a significant effort in the recent years in this field.¹⁻⁴ Gold single crystal
41
42 terminations are often adopted for their inertness to support the growth of 2D supramolecular
43
44 architectures. In particular, on the Au(111) substrate, when suitable tectons⁵ are used, the
45
46 molecule-substrate coupling is relatively weak, and manifold synthons⁶ involving non-covalent⁷⁻
47
48 ¹⁰ or metal-organic¹¹⁻¹⁵ interactions have been exploited to program the desired properties of the
49
50 final architectures. Moreover, the (111) face of gold is the most stable one, and molecular
51
52 interactions on and with this substrate are of great importance since in most applications, where
53
54 polycrystalline gold electrodes or clusters are involved, (111)-terminated facets predominate.^{16,17}
55
56
57
58
59
60

1
2
3 Despite being inert (“noble”) in its bulk form, gold exhibits rich catalytic properties and ligand
4 chemistry when in the form of small clusters composed by tens of atoms down to single atoms,
5 where gold is under-coordinated with respect to its bulk form.^{18,19} The interest in nano-gold
6 chemistry has seen a significant upswing only in the last decades, and nowadays reaches well
7 beyond fundamental research, finding valuable applications ranging from real catalysts for
8 oxidation reactions up to radiosensitization agents in cancer therapy.^{20,21} In particular,
9 heterogeneous catalysts based on highly dispersed gold have been widely investigated, and a
10 remarkable understanding of the structure-activity relationship at the nanoscale, as well as of the
11 role of the catalyst support, has been achieved in the last twenty years.^{18,22–24}

12
13
14
15
16
17
18
19
20
21
22
23
24
25 At the intersection between these two seemingly opposite worlds, i.e. the inertness of gold
26 substrates and the nanoscale reactivity of gold clusters, an exciting route opens up to novel
27 binding motifs that can encode specific properties of the supramolecular assemblies, based on
28 gold adatoms as molecular linkers. In fact, on the Au(111) surface, low-coordinated atoms are
29 natively available, since the higher density of gold atoms in the first atomic layer induces a
30 periodic displacement of the atoms out of the surface plane along the soliton walls of the
31 herringbone reconstruction.^{25,26} On this surface, extraction and stabilization of native gold
32 adatoms can be induced by interaction of organic molecules with the Au(111) surface, as
33 observed for instance with molecules containing cyano (CN) groups,^{14,15,27} organophosphorus
34 compounds,^{28,29} porphyrin or phthalocyanine derivatives^{30–32} and molecules containing very
35 electronegative substituents such as chlorine³³ or sulfur.^{34,35} Apart from thiols (R-SH), that are
36 known to induce deep restructuring of the gold surface by covalently binding to this substrate,<sup>36–
37
38
39
40
41
42
43
44
45
46
47
48
49
50
51
52
53
54
55
56
57
58
59
60</sup>
40 to our knowledge there are only few examples where 2D or 1D supramolecular architectures
are stabilized by native gold adatoms as linkers. In these cases, the Au adatoms appear to play

1
2
3 the well-known role of transition metal linkers, where reported substituents are often
4
5 distinctively electronegative.^{1,41,42} An alternative linkage method that has been recently explored
6
7 involves alkali metal linkers.⁴³ Together with providing tunable interfacial electronic
8
9 properties,⁴⁴ they also allow more flexible bonding geometries due to the ionic character of the
10
11 metal-molecule interaction, in contrast to the directional coordination enforced by the shape of
12
13 the transition metal *d* orbitals.^{1,13} Gold can be seen as a half-filled *s* shell element, in analogy to
14
15 alkali metals: this suggests the idea that under-coordinated gold adatoms could also display ionic
16
17 behavior, particularly when interacting with polarized but neutral molecules, although this has
18
19 not been reported to date. However, the observation of such ionic gold linkers by scanning
20
21 tunneling microscopy (STM) experiments could be hindered by the small ionic radius of
22
23 oxidized Au, and by the Au linker adatoms being possibly located below the plane of the
24
25 molecular adsorbates and thereby hidden.
26
27
28
29
30

31
32 In this work, we substantiate this physical picture by depositing on a gold surface a very
33
34 simple polar molecule, dimethyl sulfoxide ((CH₃)₂SO, DMSO - see inset in Figure 1), which is
35
36 constituted by a sulfinyl (S=O) group and two methyl (CH₃) groups bound to the sulfur atom,
37
38 and it is characterized by a large dipole moment (3.96 D).⁴⁵ DMSO is an aprotic solvent,
39
40 produced as a by-product of the paper industry and widely employed both in laboratory and in
41
42 industrial processes. It finds numerous applications in the electronics industry,^{46,47} in biology and
43
44 medicine as a radio- and cryo-protective agent for cells and tissues,⁴⁸ as well as a percutaneous
45
46 drug penetration enhancer.⁴⁹
47
48
49

50
51 By means of X-ray photoelectron and near-edge absorption spectroscopy (XPS and NEXAFS),
52
53 and by extensive Low Temperature Scanning Tunneling Microscopy measurements (LT-STM)
54
55 of DMSO on Au(111) from multilayer to sub-monolayer molecular coverages, we show how the
56
57
58
59
60

1
2
3 adsorption of this molecule is characterized by the formation of characteristic molecular
4 complexes composed of three or four DMSO molecules. The latter appear in the STM images to
5
6 be linked through their negatively charged, and thus presumably mutually repelling,
7
8 terminations. This puzzling supramolecular structure has been rationalized by comparing the
9
10 experimental STM images with simulated ones, obtained by density functional theory
11
12 calculations (DFT). As it will be shown, our results clearly indicate that the majority of the
13
14 observed complexes can be accurately reproduced if and only if the negatively charged oxygen
15
16 terminations are linked by one or two Au adatoms, which are “invisible” in the STM images.
17
18
19
20
21
22
23

24 RESULTS AND DISCUSSION

25
26
27 To our knowledge, only very few experimental works have characterized the adsorption of
28
29 DMSO on metal surfaces, in ultra-high vacuum (UHV)⁵⁰⁻⁵³ or in solution^{51,54,55} environments. In
30
31 particular, on Au(100) and Au(111), the structural properties of the DMSO-gold interface have
32
33 been probed by STM, but only tentative models were put forward on the basis of poorly resolved
34
35 features in the STM images.^{51,56}
36
37

38
39 In order to characterize the adsorption of DMSO, we have first monitored the O 1s and S 2p
40
41 photoemission spectral features of films obtained by depositing the molecules at different
42
43 temperatures T_s of the Au(111) sample in the 153 K < T_s < 300 K range. Curve fitting reveals
44
45 the presence of multilayer components for T_s < 193 K (top spectra in Figure 1) whereas a
46
47 decreasing coverage starting from the full monolayer is observed in the 193 K < T_s < 300 K
48
49 range. It is to be noted that, in the latter temperature range, both S 2p and O 1s spectra are always
50
51 characterized by a single component (bottom spectra of Figure 1), and no significant changes in
52
53 the profile shapes are observed with decreasing coverage. In the S 2p spectra, minor features are
54
55
56
57
58
59
60

1
2
3 visible below 165 eV, related to X-ray induced damage, as discussed in the Supporting
4 Information. In Figure 1, the deconvolution profiles obtained by the fitting procedure highlight a
5
6 binding energy shift between the monolayer (blue) and multilayer (black) components, arising
7
8 from the screening effect of the metallic substrate.
9
10
11

12
13
14
15 The shift has comparable values, within 0.1 eV, for both the S 2*p* and O 1*s* features. Both the S
16 and O atoms of the DMSO molecule have an electron lone pair and can therefore act as electron-
17 donors in binding to the substrate or to an adjacent molecule. In the latter case, as compared to a
18 non-interacting molecule, an increase in the binding energy of the donating atom is expected. On
19 these bases, in an early paper, Su and Faller⁵⁷ measured the difference between the O 1*s* and S 2*p*
20 binding energies, ΔE_b , for several metal-DMSO complexes, attempting to determine from this
21 quantity whether the metal-molecule bonding occurred through the oxygen atom, the sulfur atom
22 or both. This method was adopted to rationalize the XPS data for the adsorption of DMSO on
23 Au(100) and Pt(111),^{52,55} where bi- and mono-dentate configurations have been found,
24 respectively. By adopting this approach, the change in ΔE_b we found ($\approx 0.1\text{eV}$ – not significant
25 within our errors) suggests that, as it occurs on the Au(100) surface, also in the Au(111) case
26 DMSO adsorbs interacting with both its donor terminations to the metal. However, an important
27 aspect, which was not discussed in the cited works, has also to be considered. Indeed, the supra-
28 molecular assembly at both monolayer and multilayer stages, can be driven by the formation of
29 intermolecular hydrogen bonds, which affects the binding energy of the termination involved in
30 the interaction. If we assume that the structure of the DMSO multilayer resembles the crystalline
31 phase, where oxygen-methyl interactions are present,⁵⁸ a shift towards higher binding energies is
32 expected in addition to the screening effect of the substrate. The proper reference value of ΔE_b
33
34
35
36
37
38
39
40
41
42
43
44
45
46
47
48
49
50
51
52
53
54
55
56
57
58
59
60

1
2
3 for a non-interacting DMSO molecule should therefore be provided from spectra acquired in the
4 gas phase, which are not available. Moreover, the O-CH₃ affinity could also drive the assembly
5 of the monolayer phase. These observations indicate that it is not possible to unambiguously
6 infer a bi-dentate DMSO-metal bonding from the observed small ΔE_b , and therefore call for
7 further investigations to characterize the nature of the molecule-metal and molecule-molecule
8 interactions.
9

10
11 In order to tackle this question, we also investigated the DMSO adsorption geometry at the
12 monolayer stage by means of NEXAFS measurements. Figure 2 reports the O 1s light
13 polarization-dependent NEXAFS spectra, measured on a DMSO monolayer grown at 213 K. The
14 fit of the curves reveals the presence of distinct components, showing a clear dichroic effect, thus
15 suggesting that the molecules adsorb on the surface with preferential orientation. A detailed
16 discussion with a tentative assignment of all the main peaks of the spectra is provided in the
17 Supporting Information, on the basis of the few works present in the literature regarding the
18 electronic structure of DMSO empty states. It is to be noted that similar conclusions can be
19 drawn from NEXAFS spectra acquired at higher temperatures (also shown in the Supporting
20 Information).

21
22 Our spectra resemble the ones taken in both the gas⁵⁹ and liquid phase,⁶⁰ apart from a finer
23 structure observable in our case, possibly due to the fact that in both non-solid phases the
24 molecules are randomly oriented and dichroic effects are not measurable.
25
26

27
28 In a nutshell, comparison with gas phase spectra^{60,61} identifies peak 3 (532.7 eV) as due to a
29 transition from the O 1s to the LUMO, which has a π^* character, and is expected to have
30 maximum intensity when the photon polarization is perpendicular to the S=O bond. Conversely,
31
32
33
34
35
36
37
38
39
40
41
42
43
44
45
46
47
48
49
50
51
52
53
54
55
56
57
58
59
60

1
2
3 peak 4 (533.5 eV) shows opposite polar dependence and can be assigned to the σ^* transition of
4 the same bond. By comparing the intensities of this peak at the two polarization angles, we
5
6 determined that the S=O bond is tilted by $25^\circ \pm 10^\circ$ with respect to the surface plane.⁶²
7
8
9

10 Summarizing the information obtained from XPS and NEXAFS, on one side, XPS indicates
11 that DMSO could possibly interact with the metal both *via* the S and O atoms, whereas the role
12 of hydrogen bonding remains to be assessed. On the other, at the same time, NEXAFS reveals
13 that the S=O bond appears to be significantly raised from the surface plane. These two
14 apparently conflicting findings call for a deeper investigation of the adsorption of DMSO, and in
15 order to shed light on this point we performed high-resolution LT-STM imaging of molecular
16 layers.
17
18
19
20
21
22
23
24
25
26

27 Due to the weak bonding of the molecules in the multilayer, STM imaging could not be carried
28 out on this phase. Conversely, the structure of the monolayer phase, obtained by annealing the
29 multilayer at 193 K, could be readily imaged and is discussed in the Supporting Information.
30 Here we focus on the sub-monolayer phases. Interestingly, after annealing the monolayer phase
31 to 233 K, thereby desorbing a large part of the DMSO molecules, the surface appears as shown
32 in the STM image in Figure 3a. From the high-resolution insets (Figure 3b and c), the features
33 corresponding to the molecular structure of DMSO can be straightforwardly identified: the two
34 brighter protrusions correspond to the methyl groups, whereas the less intense one can be
35 assigned to the oxygen atom. The appearance also suggests that the molecule is sitting in an
36 “inverted umbrella” geometry, *i.e.* with the S atom directly interacting with the Au surface. From
37 these considerations, the dominant structural motif of this layer appears to be a complex of four
38 DMSO molecules (hereafter referred to as *square*), together with a smaller number of isolated,
39 single DMSO molecules.
40
41
42
43
44
45
46
47
48
49
50
51
52
53
54
55
56
57
58
59
60

1
2
3
4
5
6 Within the *square* complex, it appears that DMSO favors a geometry where the oxygen atoms
7 are located close to each other, a configuration that should intuitively be relatively unstable, due
8 to mutual repulsion of the oxygen atoms, even though a weak attractive interaction between the
9 methyl groups and the oxygen atoms of adjacent molecules could instead favor the stability of
10 the complex. In order to investigate the stability of the *squares*, we performed extensive
11 manipulation experiments, both by scanning at high bias voltages (*i.e.* within 3 V) and by
12 applying voltage pulses on top of the complexes.
13
14
15
16
17
18
19
20
21

22 What we found is that the *square* can be easily rotated as a whole on the surface plane, but it is
23 impossible to separate its constituent molecules without irreversible damage, *i.e.* the fragments
24 observed on the surface after strong manipulation attempts have completely lost the
25 characteristic appearance, in terms of size and shape, of the DMSO molecules. Therefore, the
26 interaction between the DMSO molecules within the *squares* appears to be remarkably strong
27 and dominated by the attractive CH₃-O interaction. Several examples and further details of
28 manipulation experiments are given in the Supporting Information. The issue of the stabilizing
29 interactions within the *squares* will be tackled later, after discussing the behavior of the system at
30 higher temperatures.
31
32
33
34
35
36
37
38
39
40
41
42
43
44
45

46 Subsequent annealing of the surface up to 273 K leads to a further decrease in the molecular
47 coverage and to the formation of a variety of complexes, which are summarized in Figure 4. In
48 the same figure, high resolution details of the four most common complexes are shown, whereas
49 other minor variants to these configurations can be found on the surface (less than 10% of the
50 total number of complexes). While the arrangement of the DMSO molecules within the
51
52
53
54
55
56
57
58
59
60

1
2
3 complexes in Figure 4a and 4d can be readily identified, since the shape of the single DMSO
4 molecules is evident, the complexes in Figure 4b and 4c are less trivial to understand. More
5 precisely, in the STM image in Figure 4b, three DMSO molecules can be readily identified,
6 whereas the nature of the brighter protrusion is not straightforward. Similarly, in Figure 4c, two
7 DMSO molecules can be recognized, whereas the assignment of the two brighter features needs
8 further investigation. For sake of simplicity, from now on we shall refer to the complexes in
9 Figure 4a to 4d as the *symmetric rectangle*, *asymmetric rectangle*, *chiral rectangle* and *triangle*,
10 respectively.
11
12
13
14
15
16
17
18
19
20
21

22 In order to better understand the nature of the observed bright protrusions, we have performed
23 experiments involving the manipulation of the complexes as described for the *square*. In
24 particular, Figure 5 shows the result of two subsequent voltage pulses applied at the location
25 indicated by the green markers, in a sequence of STM images acquired from the same area. As
26 can be observed, under voltage pulses, the *symmetric rectangle* can be converted back and forth
27 into the *chiral rectangle*, unambiguously confirming that the constitutive units of both *rectangles*
28 are the same, *i.e.* four DMSO molecules.
29
30
31
32
33
34
35
36
37
38
39
40

41 As shown in the Supporting Information, together with various other examples of manipulation
42 experiments, also the *asymmetric rectangle* could be converted to a *symmetric rectangle* and to a
43 *chiral rectangle*, thereby indicating that the protrusion on the side of the former complex is likely
44 a single DMSO in a different adsorption configuration.
45
46
47
48
49

50 Surprisingly enough, it appears that a common feature of all the described complexes is that
51 the oxygen atoms appear to be preferentially located close to each other, a configuration that
52 should be extremely unfavorable due to the negative charge on the oxygens. In order to
53
54
55
56
57
58
59
60

1
2
3 understand this behavior, we have carried out Density Functional Theory (DFT) calculations of
4 the structural, electronic and energetic properties of the observed DMSO complexes as well as
5 simulations of the STM images. For sake of simplicity and computational cost, we started from
6 the simplest complex, *i.e.* the *triangle*. From the experimental STM images, it can be easily
7 inferred that the complex is formed by three DMSO molecules with a measured distance of
8 approximately twice the Au lattice constant between the S atoms. DFT calculations indicate that
9 the most favorable adsorption configuration for a single adsorbed DMSO is the on-top site, with
10 the S atom bound to the metal surface. As expected from the above chemical considerations, a
11 *triangle* with all three DMSO adsorbed on top is predicted by DFT to be less stable (losing 0.13
12 eV/molecule) with respect to a single adsorbed DMSO taken as the reference configuration (1.78
13 eV/molecule). For the details of how the relevant energies are calculated, we refer the reader to
14 the discussion of Table 1 below. In this *triangle*, upon relaxation each DMSO rotates around the
15 S atom by slightly more than 30° (the DFT-optimized structure is shown in the Supporting
16 Information), in order to maximize the O-H interaction, in analogy to the behavior reported for
17 the pure crystalline form.⁵⁸ To explain the stability of the structure, we have therefore
18 hypothesized the presence of an Au adatom trapped within the complex, where it could act as an
19 acceptor for the electrons of the oxygen atoms. As a consequence of this ansatz, the *triangle*
20 becomes stable, gaining 0.25 eV/molecule with respect to single DMSO adsorption. In
21 agreement with the experimental STM data, the simulated images clearly show no protrusion
22 related to the adatom at the center of the complex, as can be seen in Figure 6d. It should be noted
23 that in the experimental STM images the *triangles* can be found pointing in both the $[11\bar{2}]$ and
24 the $[\bar{1}\bar{1}2]$ directions (see Figure 4). These two possible adsorption configurations of the *triangle*
25 are consistent with the preferred adsorption site of DMSO (on-top), and with the two possible
26
27
28
29
30
31
32
33
34
35
36
37
38
39
40
41
42
43
44
45
46
47
48
49
50
51
52
53
54
55
56
57
58
59
60

1
2
3 hollow Au sites for the adatom (*hcp* and *fcc*). Manipulation experiments described in the
4
5 Supporting Information further support this picture: the minimum lateral displacement of the
6
7 center of a *triangle*, upon switching its orientation with a voltage pulse, well agrees with the
8
9 distance between two neighboring *hcp* and *fcc* sites for the adatom.
10
11

12
13 On the basis of the same chemical considerations used for the *triangle*, the stability of the
14
15 *symmetric rectangle* can only be explained by introducing two Au adatoms, as shown in Figure
16
17 6a, gaining 0.40 eV/molecule with respect to a single adsorbed DMSO. Also in this case, the
18
19 adatoms are not visible in the experimental STM images, and the absence of protrusions related
20
21 to their presence is confirmed by the calculated image. The two adatoms are located in *fcc* and
22
23 *hcp* hollow sites, and consistently with the C_3 symmetry of the substrate, they are observed with
24
25 the long side oriented in all the three equivalent $\langle \bar{1}\bar{1}2 \rangle$ directions.
26
27

28
29 With concern to the *asymmetric rectangle* and the *chiral rectangle*, various models have been
30
31 tested, and the ones that show the best agreement with the experiment in terms of energetics and
32
33 appearance of the STM images are shown in Figure 6b and c. The energetic gain, referred to a
34
35 single adsorbed DMSO, is 0.35 eV/molecule and 0.32 eV/molecule, respectively.
36
37

38
39 In the *asymmetric rectangle* (Figure 6b), the brighter protrusion is originated by a DMSO
40
41 molecule in an “inverted” adsorption geometry, *i.e.* with the S atom pointing out of the surface
42
43 plane and the O atom interacting with the Au adatoms. As in the case of the *symmetric rectangle*,
44
45 the two adatoms are located in *fcc* and *hcp* hollow sites, and the complexes can be found on the
46
47 surface with the same orientations.
48
49

50
51 The *chiral rectangle* (Figure 6c) is again characterized by the presence of two adatoms in *fcc*
52
53 and *hcp* hollow sites. However, in this case, the two sites are almost aligned along the $[\bar{1}10]$
54
55
56
57
58
59
60

1
2
3 direction, with the adatoms located slightly off-site, giving rise to a characteristic angle of $\pm 14^\circ$
4
5 of the long side of the complex with respect to the equivalent $\langle \bar{1}10 \rangle$ directions.
6
7
8
9

10 The simulated STM images in Figure 6a-d are in good agreement with the corresponding
11 experimental images, since the morphology of the main features can be immediately identified,
12 in particular concerning the lack of features related to the presence of the adatoms. However, it is
13 also clear that the methyl groups in the simulated images always appear lower than the
14 experimental ones. This artifact can be traced back to the pseudopotential used in our
15 calculations, which underestimates the S-Au distance, inducing the methyl groups to relax to a
16 slightly lower position, thus yielding a decrease in their contrast which is not observed in the
17 experimental images (see Supporting Information for further details).
18
19
20
21
22
23
24
25
26
27
28

29 The case of the *square* complex deserves a separate discussion. Similarly to the other
30 complexes, the oxygen atoms are quite close to each other, possibly giving rise to a repulsive
31 interaction that could in principle destabilize the complex. However, in this case the molecular
32 arrangement also favors the interaction between the oxygen and the methyl groups of each
33 couple of adjacent molecules. The calculated CH-O angle in the closest H-O couple (2.5 Å) is
34 approximately 140° , and this geometry does in fact favor the formation of a hydrogen bond.⁶³⁻⁶⁵
35
36 Additionally, as mentioned above, the *square* exhibits a remarkable stability upon manipulation
37 with the STM tip. Therefore, the question arises whether or not an adatom is trapped inside the
38 complex, and the contrast of the STM images cannot address this point since we have verified
39 that the trapped adatoms, even when present, are not visible both in the experimental and
40 simulated STM images. In order to clarify this point, on one side we analyzed the distribution of
41 the characteristic orientations of the complexes with respect to the Au(111) crystallographic
42
43
44
45
46
47
48
49
50
51
52
53
54
55
56
57
58
59
60

1
2
3 directions in the experimental STM images, and on the other we carefully evaluated the
4 energetics of the different complexes as obtained by DFT.
5
6
7
8
9

10 As a starting point, we have measured the orientation of more than 1500 *square* complexes on
11 the experimental STM images, using as a reference the directions shown as blue lines in the top
12 inset of Figure 7. By taking into account both the symmetry of the substrate and the symmetry of
13 the *square* complexes themselves, the resulting angular distribution of the complexes falls within
14 0° and 60° (see Supporting Information for details on the measurement of the angles), and is
15 represented by the blue histogram in Figure 7 (left axis). It is clear that *squares* are aligned
16 around four distinct angles, namely 7°, 23°, 36° and 53° with an error of about $\pm 4^\circ$. In the same
17 graph, the green and red markers show the calculated energies of various structures composed by
18 four DMSO molecules (right axis), hypothesized as reasonable candidates for the *square*
19 complex, as a function of their characteristic angle with respect to the surface. In particular, the
20 red (green) markers correspond to the models including (excluding) the Au adatom. It is to be
21 noted that relaxation of the models corresponding to the red markers after removal of the adatom
22 consistently yielded one of the structures corresponding to the green marker.
23
24
25
26
27
28
29
30
31
32
33
34
35
36
37
38
39

40 Both analyses indicate that, at variance with the other observed complexes, the *squares* do not
41 include a central gold adatom: first of all, from the energetic point of view, it is clear that the
42 complexes with no adatom are always more stable (green markers) by more than 50 meV.
43 Second, a clearly different angular distribution should be found if the *squares* included the
44 adatoms (red markers). Details of the various models that have been simulated by DFT are
45 shown in the Supporting Information.
46
47
48
49
50
51
52
53
54
55
56
57
58
59
60

1
2
3 The adsorption geometry of DMSO within the structures obtained from DFT calculations can
4 also be compared to the one inferred from the NEXAFS spectra. As pointed out earlier, the latter
5 indicate an angle of $25^\circ \pm 10^\circ$ between the S=O direction and the surface plane, a value thus
6 fully compatible with all the calculated structures, where it lies between 25° and 32° . This result
7 can be rationalized in the context of simple chemical considerations. The sulfur atom of DMSO
8 has a tetrahedral coordination geometry, exposing an electron lone pair at the “tip” of the
9 umbrella structure that characterizes the molecule. The angle between this pair and the S=O bond
10 is roughly 110° for the free molecule. Considering that the binding to the metal substrate
11 typically occurs through the lone pair (as in the case of ammonia,⁶⁶ for instance), the expected
12 value of the angle between the S=O bond and the surface plane for the adsorbed molecule is
13 about 20° , in agreement with our results.
14
15
16
17
18
19
20
21
22
23
24
25
26
27
28

29 It is to be noted that we have no direct information to pinpoint the process by which the
30 DMSO complexes form, in particular concerning the actual origin of the adatom(s) in the
31 complexes. However, in the temperature range where we observe adatoms trapped within
32 complexes (*i.e.* above 233 K), it is well known that native gold adatoms can detach from step
33 edges, diffuse along them and across the surface itself, as well as be extracted from the
34 herringbone reconstruction and elbow sites.^{37,67,68} Moreover, it is also well established that
35 molecular adsorption, especially involving very electronegative species, can significantly
36 promote such processes.^{37,69} In contrast to thiols and other molecules that interact strongly with
37 gold, in our case no lifting of the herringbone reconstruction was ever observed, likely because
38 the interaction of DMSO with gold is comparatively weaker (no covalent bonding occurs
39 between the molecule and the metal).
40
41
42
43
44
45
46
47
48
49
50
51
52
53
54
55
56
57
58
59
60

Table 1. Calculated average adsorption (E_{ads}) and cohesion energies (E_{coh}) per DMSO molecule of the various molecular complexes (energies in eV).

species	E_{ads}	E_{coh}
single DMSO	1.78	-
<i>square</i>	1.82	0.05
<i>triangle</i>	2.02	0.25
<i>symm. rectangle</i>	2.17	0.40
<i>chiral rectangle</i>	2.09	0.32
<i>asymm. rectangle</i>	2.11	0.35

Table 1 shows the calculated average adsorption E_{ads} and cohesion E_{coh} energies per DMSO molecule of the various molecular complexes.

The adsorption energies have been calculated as:

$$E_{ads}(n) = -\frac{1}{n} [E(nDMSO/sub) - n \times E(DMSO) - E(sub)]$$

where *sub* indicates the substrate, *i.e.* the clean Au(111) surface, for the single DMSO and the *square*, or the surface with one or two Au adatoms, for the *triangle* and the *rectangles*; *nDMSO* indicates a DMSO complex with *n* molecules; $E(nDMSO/sub)$, $E(DMSO)$ and $E(sub)$ indicate the energies of the total system (adsorbed complex and substrate), of a gas-phase, isolated DMSO molecule and of the substrate, respectively. The cohesion energy per molecule, defined as

$$E_{coh}(n) = E_{ads}(n) - E_{ads}(1)$$

1
2
3 indicates the energy gain per DMSO molecule in the most stable adsorption configurations of a
4 complex with respect to the adsorption of the individual molecule(s) on the bare Au(111)
5 surface.
6
7
8
9

10 The energetics of the various complexes can help to rationalize the experimental observations.
11 The least stable species is the single DMSO molecule (1.78 eV/molecule), that was in fact
12 observed in rare cases. The *square* complex (1.82 eV/molecule) is more stable than the single
13 adsorbed molecule, and is by far the dominant structure, together with the monolayer phase, at
14 temperatures below 233 K (see Figure 3a). This is apparently in contrast with the fact that all the
15 other complexes are significantly more stable than the *square* itself, and should therefore
16 dominate the surface. However, as shown above, strong energetic and structural evidence
17 indicate that this particular complex is the only one not entrapping one or more Au adatoms. It is
18 reasonable to assume that at temperatures below 233 K a decreased availability of gold adatoms
19 prevents the formation of *triangles* and *rectangles*, and therefore favors the formation of the
20 *squares*. This consideration further strengthens the conclusion that no adatoms are trapped inside
21 the *squares*.
22
23
24
25
26
27
28
29
30
31
32
33
34
35
36
37

38 The cohesion energies reported in Table 1 indicate that the presence of the adatoms in
39 *triangles* and *rectangles* plays a relevant role in the stability of the complexes: molecule-
40 molecule and molecule-adatom interactions (E_{coh}) account for 15% to 18% of their adsorption
41 energies E_{ads} . This stabilization effect of the adatoms is also reflected in the fact that desorption
42 of DMSO becomes more costly at increasing temperatures, as shown in the Supporting
43 Information. Conversely, in the *squares*, E_{coh}/E_{ads} is only 3%, consistently with the weaker
44 molecule-molecule hydrogen bonding.
45
46
47
48
49
50
51
52
53
54
55
56
57
58
59
60

1
2
3 DFT calculations also reveal that a peculiar re-distribution of the electron density occurs
4 around the Au adatom, as shown for the *triangle* by the charge density transfer plots in Figure 8.
5
6 The latter have been calculated as $\rho_{tot}(\mathbf{r}) - \rho_{sub}(\mathbf{r}) - \sum \rho_{mol}(\mathbf{r})$, where $\rho_{tot}(\mathbf{r})$ is the charge
7
8 density of the total system, $\rho_{sub}(\mathbf{r})$ the density of the gold substrate including an isolated
9
10 adatom, and $\sum \rho_{mol}(\mathbf{r})$ the density of three non-interacting DMSO molecules in gas phase.
11
12
13
14
15
16
17

18 Namely, the density depletion (blue lobe) occurring at the gold adatom suggests that this atom
19
20 displays a significant degree of cationic behavior. This is confirmed by the calculation of the
21
22 atomic Löwdin charges:⁷⁰ even in the absence of DMSO co-adsorption, a single Au adatom in
23
24 the hollow position is always slightly positively charged ($\approx -0.21e^-$) with respect to an atom of
25
26 the surface layer, by donating electronic charge to the nearest neighbor surface Au atoms. In the
27
28 presence of a DMSO complex, the adatom recovers only part of its electronic charge (\approx
29
30 $+0.08e^-$ relative to the single adatom) and rearranges the occupation of its *s*, *p* and *d* orbitals.
31
32
33 Moreover, at the same time, an increase in the electronic charge occurs on its second nearest
34
35 neighbor surface Au atoms, which are directly interacting with the sulfur of DMSO. The oxygen
36
37 atoms surrounding the adatom are polarized in a characteristic double peak-trough pattern: this
38
39 charge rearrangement pattern favors the coordination of the oxygen terminations of DMSO with
40
41 the gold adatom, which effectively acts as ionic linker between the otherwise mutually repelling
42
43 molecular terminations. The observed charge depletion and the proximity of deep *p*-orbitals
44
45 associated with the oxygen atom ligands imply the lack of electron states available for tunneling
46
47 in the STM observations at the Au site. This is consistent with the STM images where the
48
49 adatom is indeed not visible. It is to be noted that linker adatoms which cannot be resolved in
50
51
52
53
54
55
56
57
58
59
60
STM images were also reported in other works, and this effect was accompanied by a reduction

1
2
3 of the occupation of the adatom states upon surface complexation.^{32,41} It is important to remark
4 that we have carried out extensive imaging on the complexes at various sample bias voltages,
5 ranging from -3V up to +1V. Within this interval, no significant contrast variations could be
6 observed on the complexes, except for degradation of the resolution and broadening of the
7 molecule-related protrusions. This observation gives experimental confirmation that no adatom-
8 related electronic states are available for tunneling in the examined energy range. Measuring at
9 bias voltages outside this range yielded very unstable imaging and easily induced changes in the
10 complexes, even at very low tunneling current setpoints (≈ 1 pA), pointing out to possible, strong
11 interactions between the tip-sample electric field and the molecular dipole. Eventually, it is to be
12 noted that also the simulated images show no relevant contrast variation within the above
13 mentioned bias range, and the adatom-projected density of states is negligible in the
14 corresponding energy interval.
15
16
17
18
19
20
21
22
23
24
25
26
27
28
29
30

31 Our finding of a significant charge redistribution around the presumably entrapped adatoms is
32 analogous to what observed by Pawin *et al.* for 9,10-anthracenedicarbonitrile on Cu(111), where
33 a similar effect occurs.⁷¹ Such charging effect could explain the reported increase in the
34 reactivity of Au(111) surfaces covered by PDI metal-organic frameworks with respect to CO₂
35 and CO adsorption, compared to the bare Au(111) surface.^{72,73} Notably, evidence has been found
36 that charging is at the origin of the reactivity of small gold nanoclusters on metal oxide surfaces,
37 for instance in reactions involving CO.⁷⁴⁻⁷⁷
38
39
40
41
42
43
44
45
46
47

48 Finally, we observe that the ionic character of the DMSO-adatom interaction is consistent with
49 the average Au(adatom)-O distance, which is approximately 2.6 Å, which is 30% larger than the
50 same distance in related oxo-gold compounds (~ 2.0 Å), where the Au-O bond is mainly
51 covalent.⁷⁸
52
53
54
55
56
57
58
59
60

1
2
3 A final comment is also due regarding the interpretation of the XPS spectra by the Su and
4
5
6 Faller method mentioned above, according to which, from a negligible shift in ΔE_b (as we
7
8 observe) a bidentate binding mode (S-metal and O-metal) would be expected at all the
9
10 temperatures we have characterized. In contrast to this conclusion, our STM and DFT results
11
12 indicate that at temperatures below 233 K there is no oxygen-metal bonding, but only O-CH₃
13
14 hydrogen bonds are formed. This observation points out to a limited applicability of the Su and
15
16 Faller method, primarily because it does not consider the possibility of types of S- or O-
17
18 interactions other than with the metal itself. In fact, in our case, it is evident that a similar shift in
19
20 ΔE_b can be induced by O-metal or O-CH₃ interactions.
21
22
23
24
25
26

27 CONCLUSIONS

28
29 In the present work, we have shown that there is a mutual stabilization between a common,
30
31 polar molecule, DMSO, and native, positively charged adatoms on the Au(111) surface. The
32
33 existence of these adatoms, for which no directly related features are visible in the experimental
34
35 data, is strongly supported by the agreement between the measured and simulated STM images,
36
37 as well as by the observed stability of the complexes, that would remain otherwise unexplained.
38
39 These adatoms act as ionic linkers between the molecules, a behavior reported up to now only
40
41 for alkali metal linkers. The broader interest of any such mechanism stems from the evidence
42
43 that even at low coverage, fabricating discrete structures with high size selectivity can be
44
45 achieved by exploiting more than just attractive short range intermolecular interactions (i.e., van
46
47 der Waals, or H-bonding). In particular, it is gradually becoming clear that monodisperse cluster
48
49 populations can be obtained if interactions of electrostatic nature are also present, as, for
50
51 instance, repulsive interactions between parallel dipoles which act on a longer range.⁷⁹
52
53
54
55
56
57
58
59
60

1
2
3 The observed mutual stabilization of DMSO and Au is likely related to the strong dipole
4 moment of the molecule and the strong electronegativity of its constituents: further investigations
5 are envisioned on the specific role of the sulfinyl group which could be exploited as a functional
6 group to drive the assembly of more complex tectons through the described electrostatic linkage
7 scheme, based on non-destructive extraction/stabilization of native metal atoms from the
8 substrate.
9
10

11
12
13 The nanoscale properties of the Au-DMSO interface are also of great relevance in
14 electrochemistry and, more generally, wet chemistry. For instance, a relatively strong DMSO-Au
15 binding, as originated from our observed bidentate configuration, was hypothesized as a possible
16 origin of the unusual behavior of liquid DMSO at noble metal electrodes.^{55,56,80} Very recently,
17 the ability of DMSO to act as a “functional solvent” in the synthesis of metal nanoparticles,
18 advantageously providing in a single solvent the ability to both solvate and stabilize the gold
19 aggregates, was tentatively explained by Duggan *et al.* with an enhanced S- and O- coordination
20 to gold, on the basis of FT-IR spectra.⁸¹ Clearly, a generalization of our results to the mentioned
21 cases, where liquid-solid interfaces are involved, is far from straightforward, but further
22 investigations at the liquid DMSO-Au interface could benefit from our findings.
23
24
25
26
27
28
29
30
31
32
33
34
35
36
37
38
39
40
41
42

43 METHODS

44
45 The Au(111) surface was cleaned by repeated Ne⁺ or Ar⁺ sputtering at 500 eV at room
46 temperature for 20 min followed by annealing at 873 K for 20 min. Dimethyl sulfoxide (Sigma-
47 Aldrich, anhydrous, ≥ 99%), was dosed on the Au sample by backfilling the UHV chamber
48 through a leak valve connected to a glass vial, where DMSO was transferred under nitrogen
49 atmosphere to prevent water contamination. Before dosing in the UHV chamber, DMSO was
50
51
52
53
54
55
56
57
58
59
60

1
2
3 thoroughly cleaned by means of several freeze-pump-thaw cycles. The DMSO adsorption phases
4
5 were prepared by exposing the sample held at 153 K to a background pressure of DMSO of
6
7 about 4×10^{-6} Pa for about 15 s. This preparation consistently yielded a multilayer phase.
8
9 Monolayer and sub-monolayer phases were then prepared by simply heating the multilayer phase
10
11 or by dosing at saturation at a specific sample temperature. We verified that no difference could
12
13 be observed in the final surface by using the two alternative preparation methods.
14
15

16
17 **Scanning Tunneling Microscopy:** low temperature STM measurements were carried out with
18
19 an Omicron LT-STM system, at a temperature of approximately 4 K. The microscope is hosted
20
21 in a UHV chamber, operating at a base pressure of about 1×10^{-8} Pa. Images were acquired in
22
23 the constant current mode, with the bias voltage applied to the sample and the tip at ground.
24
25 Electrochemically etched tungsten tips were used. STM images were processed by subtracting a
26
27 background plane to correct for the sample tilting.⁸² The applied enhancements consist of B-
28
29 spline resampling, to increase the sample count, and mild Gaussian filtering, to remove high
30
31 frequency noise components.
32
33
34
35

36
37 **Photoelectron spectroscopy:** XPS and NEXAFS measurements were carried out at the
38
39 ALOISA beamline of the ELETTRA synchrotron light source (Trieste, Italy).⁸³ O 1s and S 2p
40
41 XPS spectra were acquired at $h\nu = 650$ eV with an overall resolution of 0.35 eV. The binding
42
43 energy scale has been calibrated with respect to the bulk spectral component of the Au $4f_{7/2}$ peak
44
45 at 84.0 eV.⁸⁴ NEXAFS spectra were acquired in electron partial yield with a photon energy
46
47 resolution of 0.15 eV.
48
49

50
51 **Theoretical calculations:** DFT calculations were performed with the plane-wave
52
53 pseudopotential package QUANTUM ESPRESSO,⁸⁵ using ultrasoft pseudopotentials⁸⁶ with a
54
55 wave function (charge) energy cutoff of 408 eV and a GGA-PBE⁸⁷ exchange-correlation
56
57
58
59
60

1
2
3 functional. Since van der Waals interactions play a non-negligible role in self-assembled organic
4 structures, we adopted the semiempirical dispersion-corrected DFT (DFT-D) method proposed
5 by Grimme,⁸⁸ recently implemented in the QE package⁸⁹ and successfully used by Casarin *et al.*
6 to determine the adsorption energetics of iron phthalocyanine on Ag(110).⁹⁰ Brillouin-zone
7 sampling included two k points in x and y directions, and only one in z direction, perpendicular
8 to the surface. The Au(111) surface was modeled with three layers for the simulations of the
9 DMSO complexes and four layers for the monolayer simulation (see Supporting Information),
10 allowing a vacuum (adlayer – surface) distance of ≈ 1.2 nm. The bottom layer of the surface
11 was kept fixed at the bulk Au calculated values to mimic the behavior of the metal substrate. In
12 the presence of the surface, only forces acting on the top Au layer and the molecular adlayer
13 atoms were relaxed. Forces were relaxed up to 0.26 eV/Å.
14
15
16
17
18
19
20
21
22
23
24
25
26
27
28

29
30 STM images were simulated within the Tersoff-Hamann approximation according to which the
31 tunneling current is proportional to the energy-Integrated electronic Local Density Of States
32 (ILDOS).⁹¹ In order to mimic the constant-current experimental STM images we map an ILDOS
33 iso-surface lying within a certain height range over the surface. All the images in this work were
34 simulated at a bias of 100 mV, at an ILDOS value for the iso-surface of $4 \times 10^{-3} \text{ nm}^{-3}$, lying at
35 an average distance of approximately 0.5 nm from the first atomic layer. Ball models are
36 rendered with the XCrySDen, Avogadro and POV-Ray software packages.⁹²⁻⁹⁵
37
38
39
40
41
42
43
44
45
46
47

48 ASSOCIATED CONTENT

49
50
51 Additional STM manipulation experiments, temperature dependence of the molecular
52 complexes, further details on the X-ray spectroscopic data and the theoretical calculations. This
53 material is available free of charge *via* the Internet at <http://pubs.acs.org/>
54
55
56
57
58
59
60

1
2
3 AUTHOR INFORMATION
45
6 **Corresponding author**
78
9 * Email: dri@iom.cnr.it
10
1112
13
14
15
16 ACKNOWLEDGMENT
17

18 We gratefully acknowledge Federico Berti and Ambra Dreos for fruitful discussions on the
19 chemistry of DMSO. C. D., A. C., Z. F., and C. C. acknowledge financial support from MIUR
20 through Futuro in Ricerca – FIRB 2010 project no. RBFR10FQBL. A.D.V. acknowledges
21 support from the EPSRC grant EP/G044864/1 in the early stages of this work. S.V.
22 acknowledges computing resources made available at the CINECA HPC facility through the
23 UTS-CINECA Convention. M.P. acknowledges financial support from the Italian Ministry of
24 Foreign Affairs and International Cooperation, Directorate General for the Country Promotion
25 (Project PGR00190).
26
27
28
29
30
31
32
33
34
35
36

37
38 REFERENCES
39

- 40
41
42 (1) Barth, J. V. Molecular Architectonic on Metal Surfaces. *Annu. Rev. Phys. Chem.* **2007**,
43 *58*, 375–407.
44
45
46
47 (2) De Feyter, S.; De Schryver, F. C. Two-Dimensional Supramolecular Self-Assembly
48 Probed by Scanning Tunneling Microscopy. *Chem. Soc. Rev.* **2003**, *32*, 139–150.
49
50
51
52
53 (3) Bartels, L. Tailoring Molecular Layers at Metal Surfaces. *Nat. Chem.* **2010**, *2*, 87–95.
54
55
56
57
58
59
60

1
2
3 (4) Haq, S.; Hanke, F.; Sharp, J.; Persson, M.; Amabilino, D. B.; Raval, R. Versatile Bottom-
4 Up Construction of Diverse Macromolecules on a Surface Observed by Scanning Tunneling
5 Microscopy. *ACS Nano* **2014**, *8*, 8856–8870.
6
7

8
9
10
11 (5) Simard, M.; Su, D.; Wuest, J. D. Use of Hydrogen Bonds to Control Molecular
12 Aggregation. Self-Assembly of Three-Dimensional Networks with Large Chambers. *J. Am.*
13 *Chem. Soc.* **1991**, *113*, 4696–4698.
14
15

16
17
18
19 (6) Desiraju, G. R. Supramolecular Synthons in Crystal Engineering—A New Organic
20 Synthesis. *Angew. Chem. Int. Ed. Engl.* **1995**, *34*, 2311–2327.
21
22

23
24
25 (7) Clair, S.; Pons, S.; Seitsonen, A. P.; Brune, H.; Kern, K.; Barth, J. V. STM Study of
26 Terephthalic Acid Self-Assembly on Au(111): Hydrogen-Bonded Sheets on an Inhomogeneous
27 Substrate †. *J. Phys. Chem. B* **2004**, *108*, 14585–14590.
28
29

30
31
32
33 (8) Yokoyama, T.; Kamikado, T.; Yokoyama, S.; Mashiko, S. Conformation Selective
34 Assembly of Carboxyphenyl Substituted Porphyrins on Au (111). *J. Chem. Phys.* **2004**, *121*,
35 11993–11997.
36
37

38
39
40
41 (9) Otero, R.; Schöck, M.; Molina, L. M.; Lægsgaard, E.; Stensgaard, I.; Hammer, B.;
42 Besenbacher, F. Guanine Quartet Networks Stabilized by Cooperative Hydrogen Bonds. *Angew.*
43 *Chem.* **2005**, *117*, 2310–2315.
44
45

46
47
48
49 (10) Feng, Z.; Cudia, C. C.; Floreano, L.; Morgante, A.; Comelli, G.; Dri, C.; Cossaro, A. A
50 Competitive Amino-Carboxylic Hydrogen Bond on a Gold Surface. *Chem. Commun.* **2015**, *51*,
51 5739–5742.
52
53
54
55
56
57
58
59
60

1
2
3 (11) Dmitriev, A.; Spillmann, H.; Lin, N.; Barth, J. V.; Kern, K. Modular Assembly of Two-
4 Dimensional Metal–Organic Coordination Networks at a Metal Surface. *Angew. Chem.* **2003**,
5 *115*, 2774–2777.
6
7

8
9
10 (12) Garah, M. E.; Ciesielski, A.; Marets, N.; Bulach, V.; Hosseini, M. W.; Samori, P.
11 Molecular Tectonics Based Nanopatterning of Interfaces with 2D Metal–organic Frameworks
12 (MOFs). *Chem. Commun.* **2014**, *50*, 12250–12253.
13
14
15

16
17 (13) Stepanow, S.; Lin, N.; Barth, J. V. Modular Assembly of Low-Dimensional Coordination
18 Architectures on Metal Surfaces. *J. Phys. Condens. Matter* **2008**, *20*, 184002.
19
20
21

22 (14) Faraggi, M. N.; Jiang, N.; Gonzalez-Lakunza, N.; Langner, A.; Stepanow, S.; Kern, K.;
23 Arnau, A. Bonding and Charge Transfer in Metal–Organic Coordination Networks on Au(111)
24 with Strong Acceptor Molecules. *J. Phys. Chem. C* **2012**, *116*, 24558–24565.
25
26
27

28 (15) Yang, Z.; Corso, M.; Robles, R.; Lotze, C.; Fitzner, R.; Mena-Osteritz, E.; Bäuerle, P.;
29 Franke, K. J.; Pascual, J. I. Orbital Redistribution in Molecular Nanostructures Mediated by
30 Metal–Organic Bonds. *ACS Nano* **2014**, *8*, 10715–10722.
31
32
33

34 (16) Everitt, D. L.; Miller, W. J. W.; Abbott, N. L.; Zhu, X. D. Evolution of a Preferred
35 Orientation of Polycrystalline Grains in Obliquely Deposited Gold Films on an Amorphous
36 Substrate. *Phys. Rev. B* **2000**, *62*, R4833–R4836.
37
38
39

40 (17) Wang, Y.; Teitel, S.; Dellago, C. Melting of Icosahedral Gold Nanoclusters from
41 Molecular Dynamics Simulations. *J. Chem. Phys.* **2005**, *122*, 214722.
42
43
44

45 (18) Freakley, S. J.; He, Q.; Kiely, C. J.; Hutchings, G. J. Gold Catalysis: A Reflection on
46 Where We Are Now. *Catal. Lett.* **2014**, *145*, 71–79.
47
48
49
50
51
52
53
54
55
56
57
58
59
60

1
2
3 (19) Laguna, A. *Modern Supramolecular Gold Chemistry: Gold-Metal Interactions and*
4 *Applications*; John Wiley & Sons, 2008.
5
6

7
8
9 (20) Zhou, K.; Jia, J.; Li, C.; Xu, H.; Zhou, J.; Luo, G.; Wei, F. A Low Content Au-Based
10 Catalyst for Hydrochlorination of C₂H₂ and Its Industrial Scale-up for Future PVC Processes.
11 *Green Chem.* **2014**, *17*, 356–364.
12
13
14

15
16
17 (21) Dorsey, J. F.; Sun, L.; Joh, D. Y.; Witztum, A.; Kao, G. D.; Alonso-Basanta, M.; Avery,
18 S.; Hahn, S. M.; Al Zaki, A.; Tsourkas, A. Gold Nanoparticles in Radiation Research: Potential
19 Applications for Imaging and Radiosensitization. *Transl. Cancer Res.* **2013**, *2*, 280–291.
20
21
22

23
24
25 (22) Chen, M. S.; Goodman, D. W. The Structure of Catalytically Active Gold on Titania.
26 *Science* **2004**, *306*, 252–255.
27
28

29
30 (23) Choudhary, T. V.; Goodman, D. W. Catalytically Active Gold: The Role of Cluster
31 Morphology. *Appl. Catal. Gen.* **2005**, *291*, 32–36.
32
33
34

35
36 (24) Wittstock, A.; Bäumer, M. Catalysis by Unsupported Skeletal Gold Catalysts. *Acc. Chem.*
37 *Res.* **2013**, *47*, 731–739.
38
39

40
41 (25) Harten, U.; Lahee, A. M.; Toennies, J. P.; Wöll, C. Observation of a Soliton
42 Reconstruction of Au(111) by High-Resolution Helium-Atom Diffraction. *Phys. Rev. Lett.* **1985**,
43 *54*, 2619–2622.
44
45
46
47

48
49 (26) Barth, J. V.; Brune, H.; Ertl, G.; Behm, R. J. Scanning Tunneling Microscopy
50 Observations on the Reconstructed Au(111) Surface: Atomic Structure, Long-Range
51 Superstructure, Rotational Domains, and Surface Defects. *Phys. Rev. B* **1990**, *42*, 9307–9318.
52
53
54
55
56
57
58
59
60

1
2
3 (27) Boscoboinik, J. A.; Calaza, F. C.; Habeeb, Z.; Bennett, D. W.; Stacchiola, D. J.; Purino,
4 M. A.; Tysoe, W. T. One-Dimensional Supramolecular Surface Structures: 1,4-
5 Diisocyanobenzene on Au(111) Surfaces. *Phys. Chem. Chem. Phys.* **2010**, *12*, 11624–11629.
6
7

8
9
10
11 (28) Jewell, A. D.; Tierney, H. L.; Sykes, E. C. H. Gently Lifting Gold's Herringbone
12 Reconstruction: Trimethylphosphine on Au(111). *Phys. Rev. B* **2010**, *82*, 205401.
13
14

15
16
17 (29) Jewell, A. D.; Sykes, E. C. H.; Kyriakou, G. Molecular-Scale Surface Chemistry of a
18 Common Metal Nanoparticle Capping Agent: Triphenylphosphine on Au(111). *ACS Nano* **2012**,
19 *6*, 3545–3552.
20
21
22

23
24
25 (30) Mielke, J.; Hanke, F.; Peters, M. V.; Hecht, S.; Persson, M.; Grill, L. Adatoms
26 underneath Single Porphyrin Molecules on Au(111). *J. Am. Chem. Soc.* **2015**, *137*, 1844–1849.
27
28
29

30
31 (31) Saywell, A.; Greń, W.; Franc, G.; Gourdon, A.; Bouju, X.; Grill, L. Manipulating the
32 Conformation of Single Organometallic Chains on Au(111). *J. Phys. Chem. C* **2014**, *118*, 1719–
33 1728.
34
35
36

37
38 (32) Shi, Z.; Lin, N. Porphyrin-Based Two-Dimensional Coordination Kagome Lattice Self-
39 Assembled on a Au(111) Surface. *J. Am. Chem. Soc.* **2009**, *131*, 5376–5377.
40
41
42

43
44 (33) Zhang, H.; Franke, J.-H.; Zhong, D.; Li, Y.; Timmer, A.; Arado, O. D.; Mönig, H.;
45 Wang, H.; Chi, L.; Wang, Z.; *et al.* Surface Supported Gold–Organic Hybrids: On-Surface
46 Synthesis and Surface Directed Orientation. *Small* **2013**, 1361–1368.
47
48
49

50
51
52 (34) Jewell, A. D.; Tierney, H. L.; Zenasni, O.; Lee, T. R.; Sykes, E. C. H. Asymmetric
53 Thioethers as Building Blocks for Chiral Monolayers. *Top. Catal.* **2011**, *54*, 1357–1367.
54
55
56
57
58
59
60

1
2
3 (35) Bellisario, D. O.; Jewell, A. D.; Tierney, H. L.; Baber, A. E.; Sykes, E. C. H. Adsorption,
4 Assembly, and Dynamics of Dibutyl Sulfide on Au(111). *J. Phys. Chem. C* **2010**, *114*, 14583–
5 14589.
6
7
8

9
10
11 (36) Cossaro, A.; Mazzarello, R.; Rousseau, R.; Casalis, L.; Verdini, A.; Kohlmeyer, A.;
12 Floreano, L.; Scandolo, S.; Morgante, A.; Klein, M. L.; *et al.* X-Ray Diffraction and
13 Computation Yield the Structure of Alkanethiols on Gold(111). *Science* **2008**, *321*, 943–946.
14
15
16

17
18
19 (37) Maksymovych, P.; Voznyy, O.; Dougherty, D. B.; Sorescu, D. C.; Yates, J. T. Gold
20 Adatom as a Key Structural Component in Self-Assembled Monolayers of Organosulfur
21 Molecules on Au(111). *Prog. Surf. Sci.* **2010**, *85*, 206–240.
22
23
24

25
26
27 (38) Häkkinen, H. The Gold–sulfur Interface at the Nanoscale. *Nat. Chem.* **2012**, *4*, 443–455.
28
29

30 (39) Olmos-Asar, J. A.; Ludueña, M.; Mariscal, M. M. Monolayer Protected Gold
31 Nanoparticles: The Effect of the headgroup–Au Interaction. *Phys. Chem. Chem. Phys.* **2014**, *16*,
32 15979–15987.
33
34
35

36
37
38 (40) Olmos-Asar, J. A.; Rapallo, A.; Mariscal, M. M. Development of a Semiempirical
39 Potential for Simulations of Thiol–gold Interfaces. Application to Thiol-Protected Gold
40 Nanoparticles. *Phys. Chem. Chem. Phys.* **2011**, *13*, 6500–6506.
41
42
43

44
45
46 (41) Classen, T.; Fratesi, G.; Costantini, G.; Fabris, S.; Stadler, F. L.; Kim, C.; de Gironcoli,
47 S.; Baroni, S.; Kern, K. Templated Growth of Metal–Organic Coordination Chains at Surfaces.
48 *Angew. Chem. Int. Ed.* **2005**, *44*, 6142–6145.
49
50
51
52
53
54
55
56
57
58
59
60

1
2
3 (42) Tseng, T.-C.; Abdurakhmanova, N.; Stepanow, S.; Kern, K. Hierarchical Assembly and
4 Reticulation of Two-Dimensional Mn- and Ni-TCNQ_x (x = 1, 2, 4) Coordination Structures on a
5 Metal Surface. *J. Phys. Chem. C* **2011**, *115*, 10211–10217.
6
7

8
9
10
11 (43) Abdurakhmanova, N.; Floris, A.; Tseng, T.-C.; Comisso, A.; Stepanow, S.; De Vita, A.;
12 Kern, K. Stereoselectivity and Electrostatics in Charge-Transfer Mn- and Cs-TCNQ₄ Networks
13 on Ag(100). *Nat. Commun.* **2012**, *3*, 940.
14
15

16
17
18
19 (44) Floris, A.; Comisso, A.; De Vita, A. Fine-Tuning the Electrostatic Properties of an
20 Alkali-Linked Organic Adlayer on a Metal Substrate. *ACS Nano* **2013**, *7*, 8059–8065.
21
22

23
24
25 (45) Smallwood, I. M. *Handbook of Organic Solvent Properties*; Arnold; Halsted Press:
26 London; New York, 1996.
27
28

29
30 (46) Kvakovszky, G.; McKim, A.; Moore, J. C. A Review of Microelectronic Manufacturing
31 Applications Using DMSO-Based Chemistries. *ECS Trans.* **2007**, *11*, 227–234.
32
33

34
35
36 (47) Zhu, P.; Chen, Y.; Wang, L.; Qian, G.; Zhang, W. J.; Zhou, M.; Zhou, J. Dissolution of
37 Brominated Epoxy Resins by Dimethyl Sulfoxide To Separate Waste Printed Circuit Boards.
38 *Environ. Sci. Technol.* **2013**, *47*, 2654–2660.
39
40

41
42
43
44 (48) Ashwood-Smith, M. J. Current Concepts Concerning Radioprotective and Cryoprotective
45 Properties of Dimethyl Sulfoxide in Cellular Systems. *Ann. N. Y. Acad. Sci.* **1975**, *243*, 246–256.
46
47

48
49 (49) Thong, H.-Y.; Zhai, H.; Maibach, H. I. Percutaneous Penetration Enhancers: An
50 Overview. *Skin Pharmacol. Physiol.* **2007**, *20*, 272–282.
51
52

53
54
55 (50) Schröter, C.; Roelfs, B.; Solomun, T. The Interaction of Dimethylsulfoxide with a Gold
56 Surface. *Surf. Sci.* **1997**, *380*, L441–L445.
57
58
59
60

1
2
3 (51) Ikemiya, N.; Gewirth, A. A. Structure Sensitive Adsorption of DMSO on Au Surfaces. *J.*
4
5
6 *Phys. Chem. B* **2000**, *104*, 873–877.

7
8
9 (52) Sexton, B. A.; Avery, N. R.; Turney, T. W. A Spectroscopic Study of the Coordination of
10
11
12 Dimethyl Sulfoxide to a Platinum (111) Surface. *Surf. Sci.* **1983**, *124*, 162–174.

13
14 (53) Garwood Jr, G. A.; Hubbard, A. T. Superlattices Formed by Interaction of Polar Solvents
15
16
17 with Pt (111) Surfaces Studied by LEED, Auger Spectroscopy and Thermal Desorption Mass
18
19
20 Spectrometry. *Surf. Sci.* **1982**, *118*, 223–247.

21
22 (54) Si, S. K.; Gewirth, A. A. Complex Formation between Halogens and Sulfoxides on Metal
23
24
25 Surfaces. *Phys. Chem. Chem. Phys.* **2001**, *3*, 3325–3329.

26
27 (55) Roelfs, B.; Schröter, C.; Solomun, T. A Comparison of Metal/vacuum and
28
29
30 Metal/electrolyte Interfaces: The Au(100)/(dimethylsulfoxide) and (dimethylsulfoxide +
31
32
33 Acetonitrile) Systems. *Berichte Bunsenges. Für Phys. Chem.* **1997**, *101*, 1105–1112.

34
35 (56) Si, S. K.; Gewirth, A. A. Solvent Organization above Metal Surfaces: Ordering of
36
37
38 DMSO on Au. *J. Phys. Chem. B* **2000**, *104*, 10775–10782.

39
40 (57) Su, C.-C.; Faller, J. W. Application of Electron Spectroscopy for Chemical Analysis to
41
42
43 the Study of Ambidentate Binding in Sulfoxide Complexes. *Inorg. Chem.* **1974**, *13*, 1734–1736.

44
45 (58) Thomas, R.; Shoemaker, C. B.; Eriks, K. The Molecular and Crystal Structure of
46
47
48 Dimethyl Sulfoxide, (H₃C)₂SO. *Acta Crystallogr.* **1966**, *21*, 12–20.

49
50 (59) Leite, T. C. M.; de Barros, A. L. F.; Ferreira, G. B.; Guerra, A. C. O.; Turci, C. C.
51
52
53 Photoabsorption Spectroscopy of Dimethyl Sulfoxide at the O1s, C1s, S2s, and S2p Regions: A
54
55
56 Comparison with Acetone. *Int. J. Quantum Chem.* **2012**, *112*, 3421–3433.
57
58
59
60

1
2
3 (60) Atak, K.; Engel, N.; Lange, K. M.; Golnak, R.; Gotz, M.; Soldatov, M.; Rubensson, J.-E.;
4
5 Kosugi, N.; Aziz, E. F. The Chemical Bond in Carbonyl and Sulfinyl Groups Studied by Soft X-
6
7 Ray Spectroscopy and Ab Initio Calculations. *ChemPhysChem* **2012**, *13*, 3106–3111.
8
9

10
11 (61) Sze, K. H.; Brion, C. E.; Tronc, M.; Bodeur, S.; Hitchcock, A. P. Inner and Valence Shell
12
13 Electronic Excitation of Dimethyl Sulfoxide by Electron Energy Loss and Photoabsorption
14
15 Spectroscopies. *Chem. Phys.* **1988**, *121*, 279–297.
16
17

18
19 (62) Stöhr, J. *NEXAFS Spectroscopy*; Springer Series in Surface Sciences; Springer--Verlag,
20
21 1992; Vol. 25.
22
23

24
25 (63) Knak Jensen, S. J.; Tang, T.-H.; Csizmadia, I. G. Hydrogen-Bonding Ability of a Methyl
26
27 Group. *J. Phys. Chem. A* **2003**, *107*, 8975–8979.
28
29

30
31 (64) Cepellotti, A.; Peronio, A.; Marchini, S.; Abdurakhmanova, N.; Dri, C.; Africh, C.; Esch,
32
33 F.; Comelli, G.; Peressi, M. NH₃–NO Coadsorption System on Pt(111). II. Intermolecular
34
35 Interaction. *J. Phys. Chem. C* **2013**, *117*, 21196–21202.
36
37

38
39 (65) Desiraju, G. R. The C–H···O Hydrogen Bond: Structural Implications and
40
41 Supramolecular Design. *Acc. Chem. Res.* **1996**, *29*, 441–449.
42
43

44
45 (66) Peronio, A.; Cepellotti, A.; Marchini, S.; Abdurakhmanova, N.; Dri, C.; Africh, C.; Esch,
46
47 F.; Peressi, M.; Comelli, G. NH₃–NO Coadsorption System on Pt(111). I. Structure of the Mixed
48
49 Layer. *J. Phys. Chem. C* **2013**, *117*, 21186–21195.
50
51

52 (67) Stoltze, P. Simulation of Surface Defects. *J. Phys. Condens. Matter* **1994**, *6*, 9495.
53
54

55 (68) Zhang, J.-M.; Song, X.-L.; Zhang, X.-J.; Xu, K.-W.; Ji, V. Atomistic Simulation of Point
56
57 Defects at Low-Index Surfaces of Noble Metals. *Surf. Sci.* **2006**, *600*, 1277–1282.
58
59
60

1
2
3 (69) Baker, T. A.; Kaxiras, E.; Friend, C. M. Insights from Theory on the Relationship
4 Between Surface Reactivity and Gold Atom Release. *Top. Catal.* **2010**, *53*, 365–377.
5
6

7
8
9 (70) Löwdin, P.-O. Quantum Theory of Many-Particle Systems. I. Physical Interpretations by
10 Means of Density Matrices, Natural Spin-Orbitals, and Convergence Problems in the Method of
11 Configurational Interaction. *Phys. Rev.* **1955**, *97*, 1474–1489.
12
13
14

15
16
17 (71) Pawin, G.; Wong, K. L.; Kim, D.; Sun, D.; Bartels, L.; Hong, S.; Rahman, T. S.; Carp,
18 R.; Marsella, M. A Surface Coordination Network Based on Substrate-Derived Metal Adatoms
19 with Local Charge Excess. *Angew. Chem. Int. Ed.* **2008**, *47*, 8442–8445.
20
21
22

23
24
25 (72) Boscoboinik, J.; Kestell, J.; Garvey, M.; Weinert, M.; Tysoe, W. T. Creation of Low-
26 Coordination Gold Sites on Au(111) Surface by 1,4-Phenylene Diisocyanide Adsorption. *Top.*
27 *Catal.* **2011**, *54*, 20–25.
28
29
30

31
32
33 (73) Feng, M.; Sun, H.; Zhao, J.; Petek, H. Self-Catalyzed Carbon Dioxide Adsorption by
34 Metal-Organic Chains on Gold Surfaces. *ACS Nano* **2014**, *8*, 8644–8652.
35
36
37

38
39 (74) Rim, K. T.; Eom, D.; Liu, L.; Stolyarova, E.; Raitano, J. M.; Chan, S.-W.; Flytzani-
40 Stephanopoulos, M.; Flynn, G. W. Charging and Chemical Reactivity of Gold Nanoparticles and
41 Adatoms on the (111) Surface of Single-Crystal Magnetite: A Scanning Tunneling
42 Microscopy/Spectroscopy Study. *J. Phys. Chem. C* **2009**, *113*, 10198–10205.
43
44
45
46

47
48
49 (75) Chrétien, S.; Metiu, H. Density Functional Study of the Charge on Aun Clusters (n=1–7)
50 Supported on a Partially Reduced Rutile TiO₂(110): Are All Clusters Negatively Charged? *J.*
51 *Chem. Phys.* **2007**, *126*, 104701.
52
53
54
55
56
57
58
59
60

1
2
3 (76) Wörz, A. S.; Heiz, U.; Cinquini, F.; Pacchioni, G. Charging of Au Atoms on TiO₂ Thin
4 Films from CO Vibrational Spectroscopy and DFT Calculations. *J. Phys. Chem. B* **2005**, *109*,
5 18418–18426.
6
7
8

9
10
11 (77) Baker, T. A.; Liu, X.; Friend, C. M. The Mystery of Gold's Chemical Activity: Local
12 Bonding, Morphology and Reactivity of Atomic Oxygen. *Phys. Chem. Chem. Phys.* **2010**, *13*,
13 34–46.
14
15
16

17
18
19 (78) Bauer, A.; Schier, A.; Schmidbaur, H. (Methyldiphenylphosphine) (trimethylsiloxy)
20 gold(I). *Acta Crystallogr. C* **1995**, *51*, 2030–2032.
21
22
23

24
25 (79) Kervyn, S.; Kalashnyk, N.; Riello, M.; Moreton, B.; Tasseroul, J.; Wouters, J.; Jones, T.
26 S.; De Vita, A.; Costantini, G.; Bonifazi, D. “Magic” Surface Clustering of Borazines Driven by
27 Repulsive Intermolecular Forces. *Angew. Chem. Int. Ed.* **2013**, *52*, 7410–7414.
28
29
30

31
32
33 (80) Borkowska, Z.; Hamelin, A. The Influence of the Crystallographic Orientation on the
34 Double Layer Parameters of the Au/dimethylsulphoxide Interface. *J. Electroanal. Chem.*
35 *Interfacial Electrochem.* **1988**, *241*, 373–377.
36
37
38

39
40
41 (81) Duggan, J. N.; Roberts, C. B. Aggregation and Precipitation of Gold Nanoparticle
42 Clusters in Carbon Dioxide-Gas-Expanded Liquid Dimethyl Sulfoxide. *J. Phys. Chem. C* **2014**,
43 *118*, 14595–14605.
44
45
46

47
48
49 (82) Nečas, D.; Klapetek, P. Gwyddion: An Open-Source Software for SPM Data Analysis.
50 *Cent. Eur. J. Phys.* **2012**, *10*, 181–188.
51
52
53

54
55 (83) Floreano, L.; Naletto, G.; Cvetko, D.; Gotter, R.; Malvezzi, M.; Marassi, L.; Morgante,
56 A.; Santaniello, A.; Verdini, A.; Tommasini, F.; *et al.* Performance of the Grating-Crystal
57
58
59
60

1
2
3 Monochromator of the ALOISA Beamline at the Elettra Synchrotron. *Rev. Sci. Instrum.* **1999**,
4
5 70, 3855–3864.

6
7
8
9 (84) Cossaro, A.; Floreano, L.; Verdini, A.; Casalis, L.; Morgante, A. Comment on “Local
10
11 Methylthiolate Adsorption Geometry on Au(111) from Photoemission Core-Level Shifts”. *Phys.*
12
13 *Rev. Lett.* **2009**, 103, 119601.

14
15
16 (85) Giannozzi, P.; Baroni, S.; Bonini, N.; Calandra, M.; Car, R.; Cavazzoni, C.; Ceresoli, D.;
17
18 Chiarotti, G. L.; Cococcioni, M.; Dabo, I.; *et al.* QUANTUM ESPRESSO: A Modular and Open-
19
20 Source Software Project for Quantum Simulations of Materials. *J. Phys. Condens. Matter* **2009**,
21
22 21, 395502.

23
24
25 (86) Vanderbilt, D. Soft Self-Consistent Pseudopotentials in a Generalized Eigenvalue
26
27 Formalism. *Phys. Rev. B* **1990**, 41, 7892–7895.

28
29
30 (87) Perdew, J. P.; Burke, K.; Ernzerhof, M. Generalized Gradient Approximation Made
31
32 Simple. *Phys. Rev. Lett.* **1996**, 77, 3865.

33
34
35 (88) Grimme, S. Semiempirical GGA-Type Density Functional Constructed with a Long-
36
37 Range Dispersion Correction. *J. Comput. Chem.* **2006**, 27, 1787–1799.

38
39
40 (89) Barone, V.; Casarin, M.; Forrer, D.; Pavone, M.; Sambri, M.; Vittadini, A. Role and
41
42 Effective Treatment of Dispersive Forces in Materials: Polyethylene and Graphite Crystals as
43
44 Test Cases. *J. Comput. Chem.* **2009**, 30, 934–939.

45
46
47 (90) Casarin, M.; Marino, M. D.; Forrer, D.; Sambri, M.; Sedona, F.; Tondello, E.; Vittadini,
48
49 A.; Barone, V.; Pavone, M. Coverage-Dependent Architectures of Iron Phthalocyanine on
50
51 Ag(110): A Comprehensive STM/DFT Study. *J. Phys. Chem. C* **2010**, 114, 2144–2153.

1
2
3 (91) Tersoff, J.; Hamann, D. R. Theory of the Scanning Tunneling Microscope. *Phys. Rev. B*
4
5 **1985**, *31*, 805–813.

6
7
8 (92) Kokalj, A. Computer Graphics and Graphical User Interfaces as Tools in Simulations of
9
10 Matter at the Atomic Scale. *Comput. Mater. Sci.* **2003**, *28*, 155–168.

11
12 (93) Avogadro: an open-source molecular builder and visualization tool. Version 1.1.1.
13
14 <http://avogadro.openmolecules.net/>
15
16

17
18 (94) Hanwell, M. D.; Curtis, D. E.; Lonie, D. C.; Vandermeersch, T.; Zurek, E.; Hutchison, G.
19
20 R. Avogadro: An Advanced Semantic Chemical Editor, Visualization, and Analysis Platform. *J.*
21
22 *Cheminformatics* **2012**, *4*, 17.

23
24 (95) Persistence of Vision Pty. Ltd (2004), Persistence of Vision Raytracer (Version 3.6),
25
26 retrieved from <http://www.povray.org/download/>
27
28
29
30
31
32
33
34
35
36

37 **Figure 1.** O 1s and S 2p spectra ($h\nu = 650$ eV) acquired on the multilayer (153 K – top spectra -
38
39 green) and on the monolayer (213 K – bottom spectra - blue) phase. The uncertainty on the
40
41 absolute binding energy values is ± 0.05 eV. Individual components, obtained from the fit, are
42
43 superimposed on the spectra. The inset shows a ball and stick model of the DMSO molecule
44
45 (yellow: sulfur, red: oxygen, grey: carbon, white: hydrogen).
46
47
48
49
50
51
52

53 **Figure 2.** Linear dichroism NEXAFS spectra at the O 1s edge for two different synchrotron light
54
55 polarizations (s polarization: parallel to the surface; p polarization: perpendicular to the surface)
56
57 of DMSO/Au(111) after annealing at 213 K. The main peaks, 3 and 4, are located at 532.7 eV
58
59
60

1
2
3 and 533.5 eV respectively. Peaks 1 and 2 are assigned to impurities or beam induced damage,
4
5 whereas peaks 5, 6 and 7 are related to oxygen Rydberg states⁵⁹ (see Supporting Information for
6
7 a discussion of the assignments).
8
9

10
11
12
13
14 **Figure 3.** (a) STM image ($12.82 \times 12.82 \text{ nm}^2$) showing the *square* complexes formed by
15
16 annealing the DMSO/Au(111) multilayer phase to 233 K. Panels (b) ($1.00 \times 1.00 \text{ nm}^2$) and (c)
17
18 ($1.60 \times 1.60 \text{ nm}^2$) are high-resolution details of a single isolated DMSO molecule and a *square*
19
20 complex, respectively. Transparent ball and stick models are superimposed to guide the eye in
21
22 the identification of the single molecules. Image parameters: (a) $V_s = 100 \text{ mV}$, $I_t = 100 \text{ pA}$; (b)
23
24 $V_s = 50 \text{ mV}$, $I_t = 100 \text{ pA}$; (c) $V_s = 100 \text{ mV}$, $I_t = 50 \text{ pA}$.
25
26
27
28
29
30
31
32

33 **Figure 4.** STM image (center - $12.94 \times 12.94 \text{ nm}^2$) showing the various complexes that form
34
35 on the surface after annealing to 273 K. (a) to (d) insets show high resolution details of
36
37 complexes: (a) the *rectangle* complex ($1.63 \times 1.99 \text{ nm}^2$), (b) the *asymmetric rectangle*
38
39 complex ($2.21 \times 1.62 \text{ nm}^2$), (c) the *chiral rectangle* complex ($2.21 \times 1.62 \text{ nm}^2$) and (d) the
40
41 *triangle* complex ($1.63 \times 1.99 \text{ nm}^2$). All images: $30 \text{ mV} < V_s < 50 \text{ mV}$, $100 \text{ pA} < I_t <$
42
43 200 pA .
44
45
46
47
48
49
50

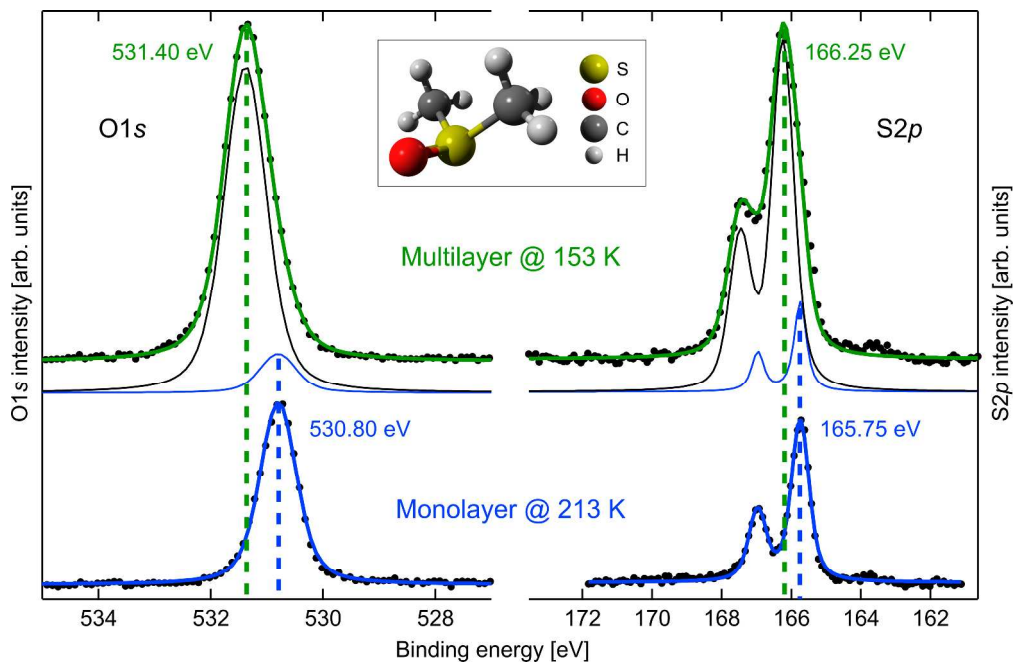
51 **Figure 5.** Sequence of STM images of the same area, showing the effect of +1.5 V voltage
52
53 pulses applied with the STM tip at the location indicated by the green marker. A *symmetric*
54
55 *rectangle* (a) is converted to a *chiral rectangle* (b) and eventually back to a *symmetric rectangle*.
56
57
58
59
60

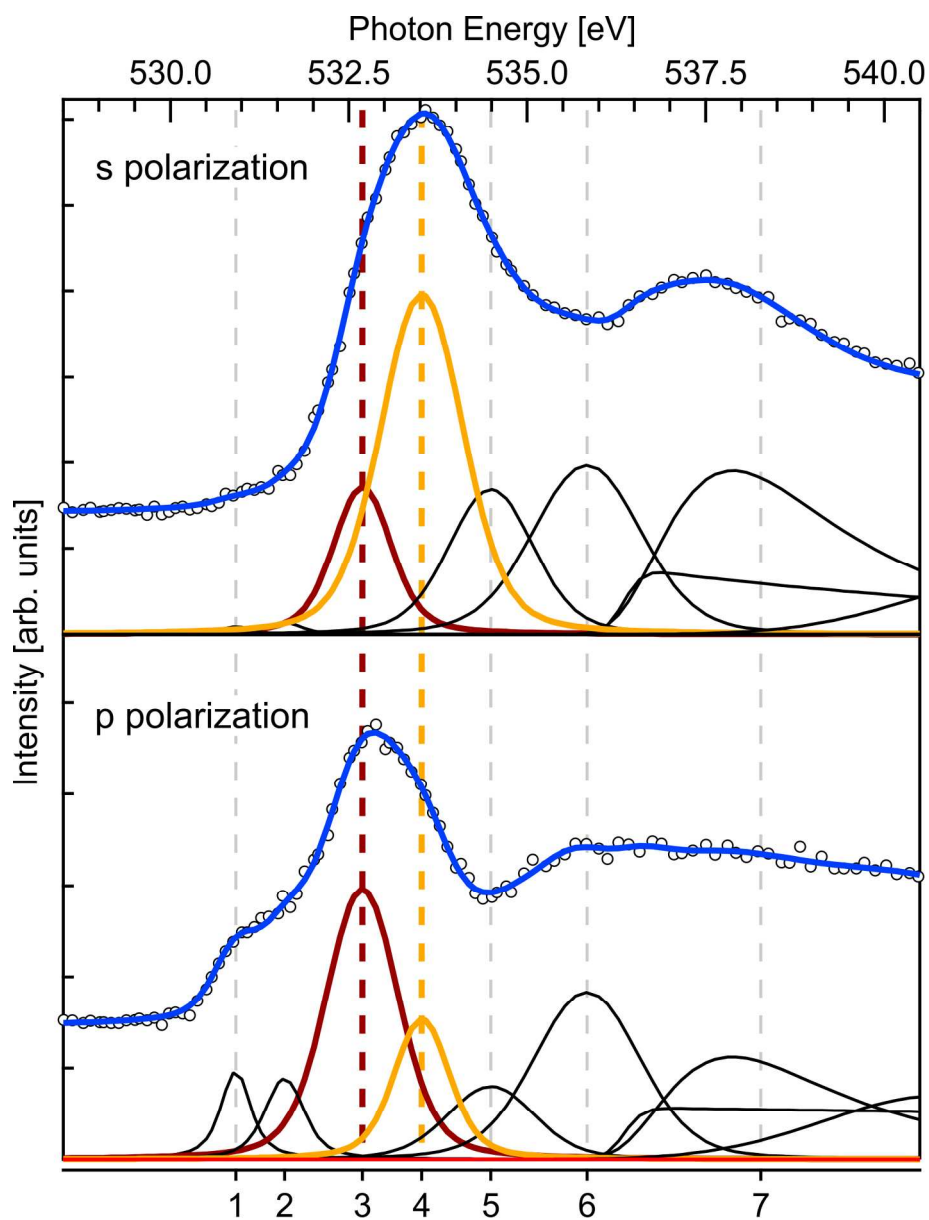
1
2
3 The *triangle* at the bottom right corner remains immobile in all three images, and acts as a
4 reference. All images: $V_s = 100$ mV, $I_t = 100$ pA, 4.20×4.20 nm².
5
6
7
8
9
10

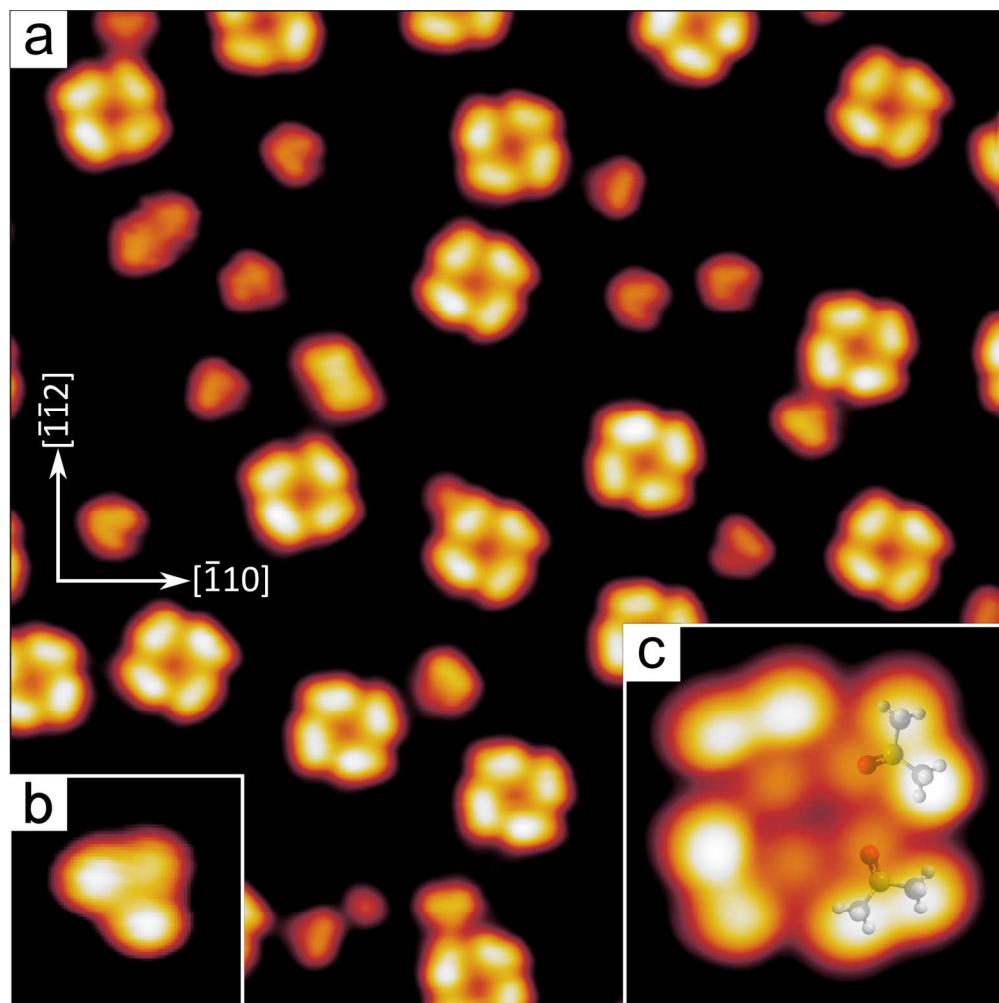
11 **Figure 6.** (a-e) STM images of the various DMSO complexes from Figures 4a-d and 3c,
12 showing the experimental (top row) and the DFT calculated images (middle row). The bottom
13 row shows ball models of the geometries obtained by DFT calculations, where the gold adatoms
14 are painted in green to ease their identification. The lateral scales of the images within each
15 column are the same, and are the same of Figure 4a-d and Figure 3c.
16
17
18
19
20
21
22
23
24
25
26
27

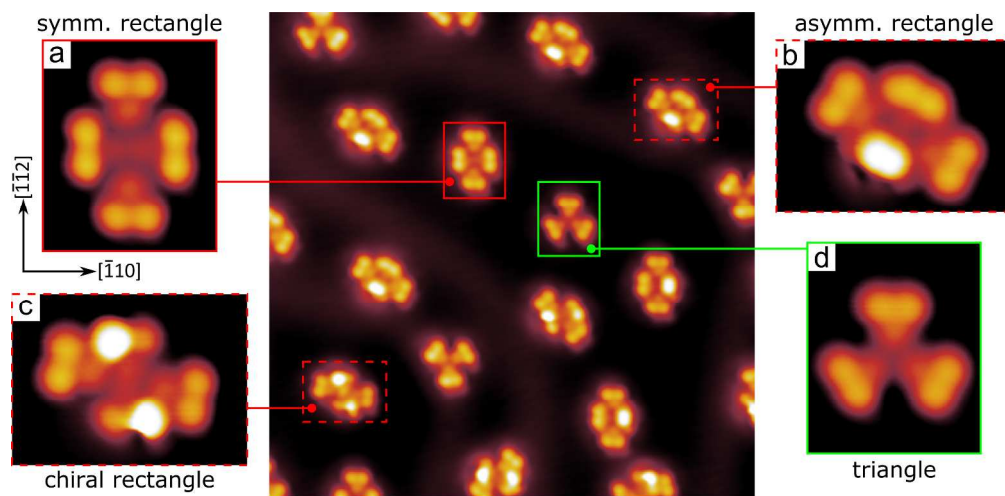
28 **Figure 7.** The experimental angular distribution of the *square* complexes (blue histogram - left
29 axis) and the adsorption energy per molecule (markers - right axis) of the possible candidate
30 models for the *square* complex with (red) and without (green) the central adatom. The thumbnail
31 above the graph shows the directions taken as a reference to determine the orientation of the
32 *square* complexes.
33
34
35
36
37
38
39
40
41
42
43

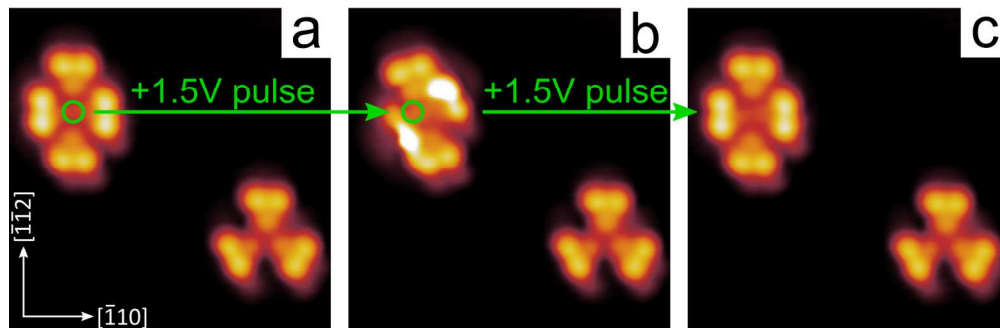
44 **Figure 8.** Top (top panel) and side (bottom panel) views of the changes in charge density around
45 a gold adatom coordinated by three DMSO molecules (*triangle* complex) on the Au(111) surface
46 with a pre-existing adatom on it. A perspective view (middle panel) is also shown. The
47 accumulation of negative charge is depicted in red, the depletion in blue. The blue lobe
48 surrounding the adatom highlights its cationic behavior.
49
50
51
52
53
54
55
56
57
58
59
60

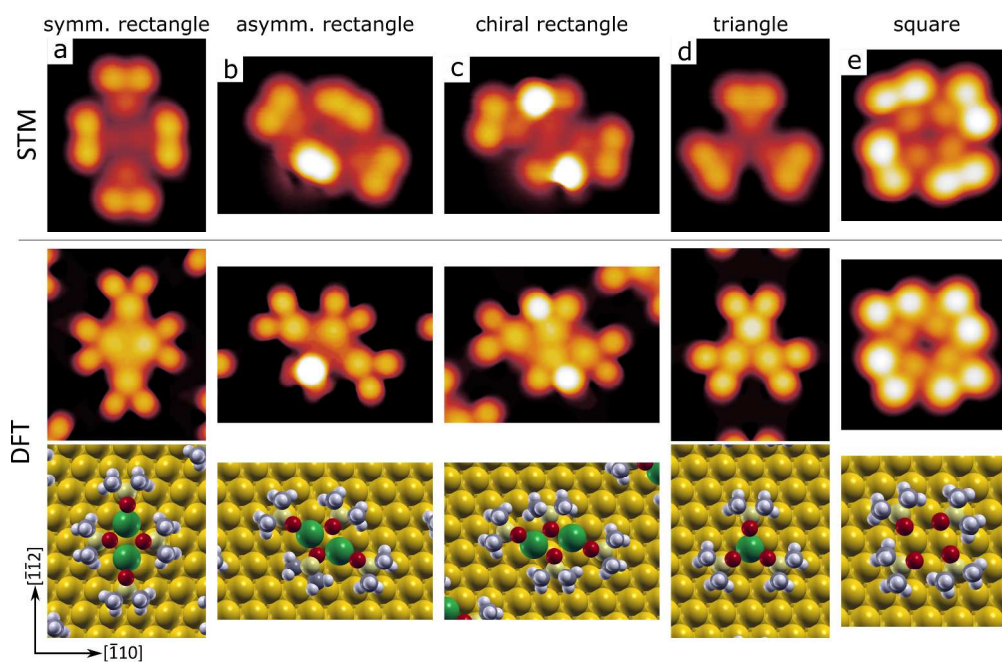


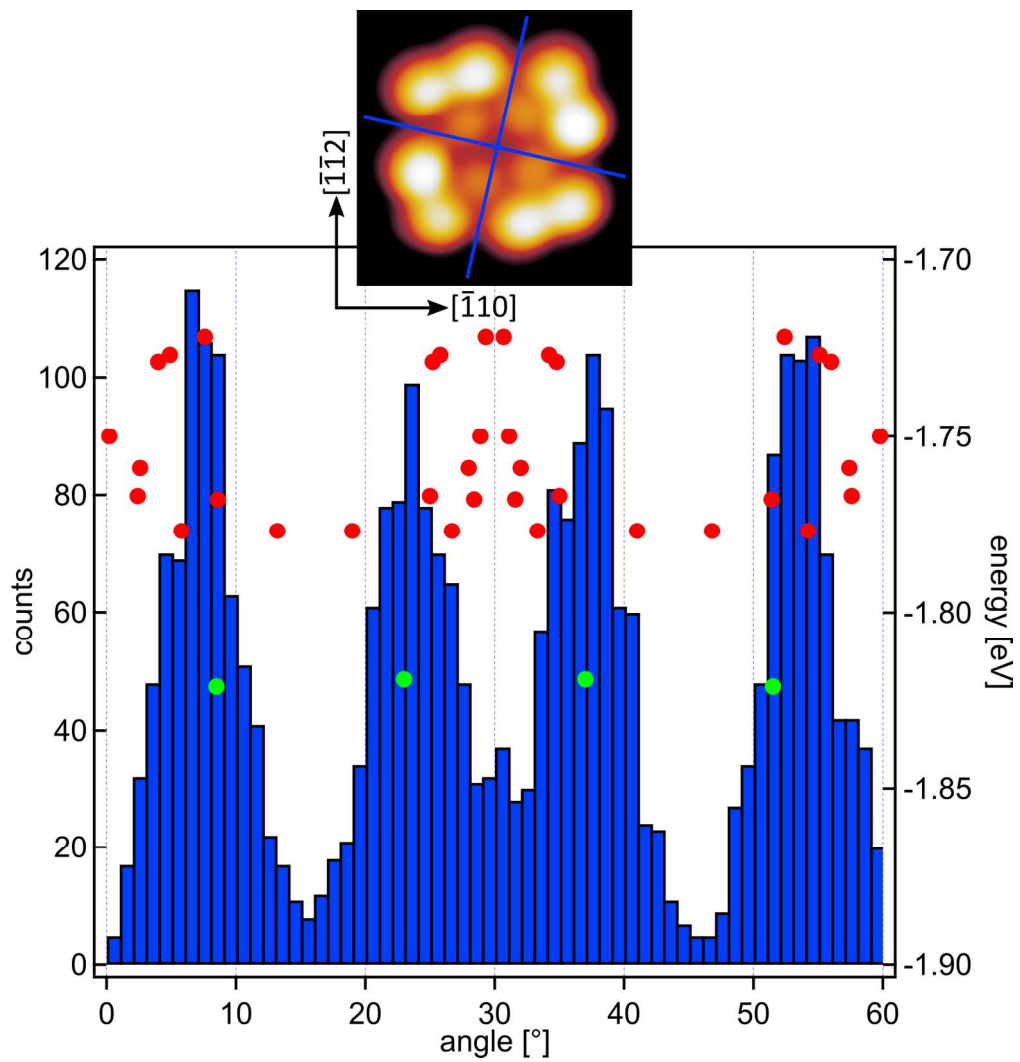


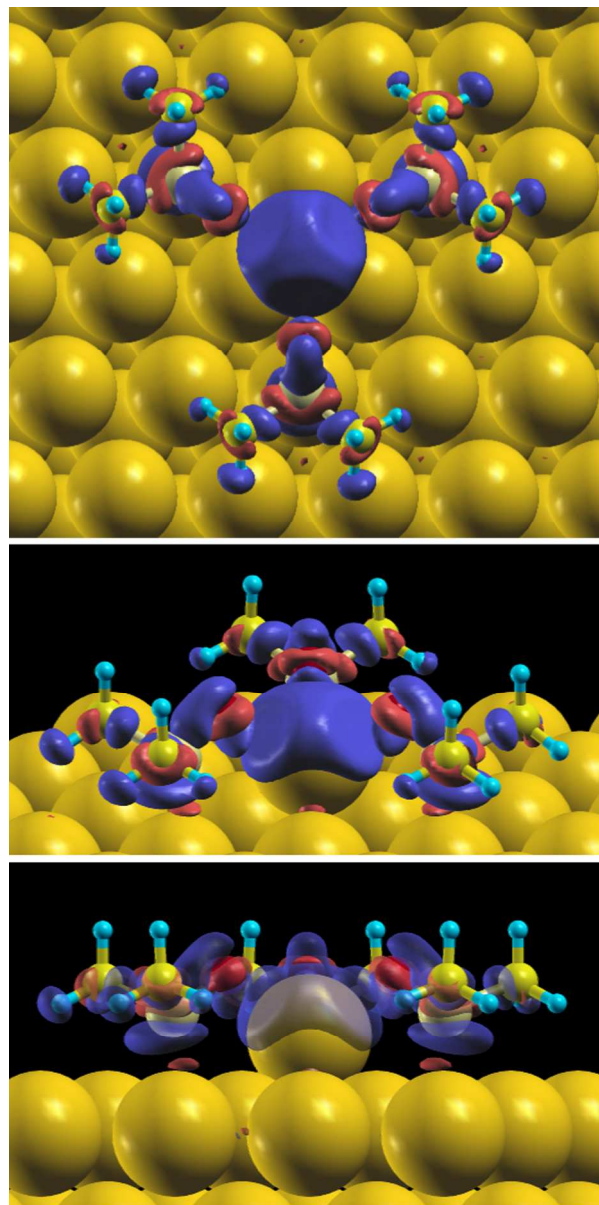












1
2
3
4
5
6
7
8
9
10
11
12
13
14
15
16
17
18
19
20
21
22
23
24
25
26
27
28
29
30
31
32
33
34
35
36
37
38
39
40
41
42
43
44
45
46
47
48
49
50
51
52
53
54
55
56
57
58
59
60

